Applied Catalysis B: Environmental 250 (2019) 408–418

Contents lists available at ScienceDirect

Applied Catalysis B: Environmental

journal homepage: www.elsevier.com/locate/apcatb

Insights into the role of singlet oxygen in the photocatalytic hydrogen peroxide production over polyoxometalates-derived metal oxides incorporated into graphitic carbon nitride framework

Shen Zhao[a], Xu Zhao[a,b,*]

[a] Key Laboratory of Drinking Water Science and Technology, Research Center for Eco-Environmental Sciences, Chinese Academy of Sciences, Beijing 100085, China
[b] University of Chinese Academy of Sciences, Beijing, 100049, China

ARTICLE INFO

Keywords:
Graphitic carbon nitride
Polyoxometalates
Photocatalytic hydrogen peroxide production
Oxygen reduction
Singlet oxygen

ABSTRACT

To develop a new strategy of enhancing the photoinduced holes (h^+) consumption to promote the photoinduced electrons (e^-) utilization for O_2 reduction to H_2O_2 and maintaining the chemical stability of g-C_3N_4-based catalysts, the hybrid catalyst of g-C_3N_4-CoWO has been prepared through the calcination of the graphitic carbon nitride (g-C_3N_4) precursor of 3-amino 1, 2, 4-triazole (3-AT) and the polyoxometalates (POMs) precursor of $(NH_4)_8Co_2W_{12}O_{42}$ (NH_4-Co_2W_{12}). The hybrid catalyst of g-C_3N_4-CoWO with well-defined and stable structure exhibits efficient catalytic performance (9.7 μmol h^{-1}) for photocatalytic H_2O_2 production in the absence of organic electron donor under visible light. The value of electrons transfer during the oxygen reduction reaction (ORR) process obtained from the Koutecky-Levich plot for g-C_3N_4-CoWO (n = 1.95) is higher than that for g-C_3N_4 (n = 1.18), suggesting that the CoWO incorporated into g-C_3N_4 framework can generate more e^- for O_2 reduction. The superoxide radicals ($^{\cdot}O_2$-) quantitative and scavenger experiments combined with the electron spin resonance (ESR) results reveal that the negative shifts of the conduction band (CB) level from g-C_3N_4 to g-C_3N_4-CoWO can enhance the single-electron reduction of O_2 to $^{\cdot}O_2$-. The h^+ and $^1O_2$ scavenger experiments results combined with the ESR results demonstrate that the CoWO incorporated into g-C_3N_4 framework can promote the oxidation of $^{\cdot}O_2$- to $^1O_2$ by h^+. The $^1O_2$ quantitative experiments results indicate that the $^1O_2$ can proceed two-electron reduction to H_2O_2. The enhanced h^+ consumption and the $^1O_2$ transferred from $^{\cdot}O_2$- can promote the photocatalytic H_2O_2 production over g-C_3N_4-CoWO. In addition, the recycle experiment results reveal that the heterogeneous g-C_3N_4-CoWO is catalytic stable.

1. Introduction

As a clean environment and green oxidant, hydrogen peroxide (H_2O_2) is convenient and safe storage and transportation in liquid form and producing water (H_2O) as the sole by-product. Therefore, it can be widely utilized in organic synthesis, environmental remediation, disinfection and one-compartment fuel cells alternative to hydrogen (H_2) [1]. However, the anthraquinone method (the Riedl-Pfleiderer process) utilized in industry catalyzed by Pd-based catalysts requires the regeneration of anthrahydroquinone by H_2 [2a], and the direct synthesis of H_2O_2 with H_2 and O_2 catalyzed by Pd or Au-Pd catalysts should pay more attention to the potentially explosive nature of H_2/O_2 mixed gases [2b]. A noble metal-free approach capable of producing H_2O_2 without H_2 is therefore desired.

$$H_2O + 1/2O_2 \rightarrow H_2O_2 \ (\Delta G^o = 117\ kJ{\cdot}mol^{-1}) \quad (1)$$

$$O_2 + 2H^+ + 2e^- \rightarrow H_2O_2 \ (0.68\ V\ vs.\ NHE) \quad (2)$$

$$O_2 + e^- \rightarrow {}^{\cdot}O_2^- \ (-0.13\ V\ vs.\ NHE) \quad (3)$$

$$^{\cdot}O_2^- + 2H^+ + e^- \rightarrow H_2O_2 \ (1.44\ V\ vs.\ NHE) \quad (4)$$

The photocatalytic H_2O_2 production method through proton-coupled electron transfer (PCET) process can meet the above requirement because it only needs H_2O, dioxygen (O_2) and light (Eq. (1)) [3]. Since the formed 1,4-endoperoxide species on the graphitic carbon nitride (g-C_3N_4) surface actually gets transformed as H_2O_2 molecule, it exhibit efficient performance for photocatalytic H_2O_2 production [[4]]. Generally, the photocatalytic H_2O_2 production over g-C_3N_4-based catalysts can process either a direct two-electron O_2 reduction (Eq. (2)) [[5]] or a

* Corresponding author at: Key Laboratory of Drinking Water Science and Technology, Research Center for Eco-Environmental Sciences, Chinese Academy of Sciences, Beijing 100085, China.
E-mail address: zhaoxu@rcees.ac.cn (X. Zhao).

https://doi.org/10.1016/j.apcatb.2019.02.031
Received 29 November 2018; Received in revised form 3 February 2019; Accepted 12 February 2019
Available online 13 February 2019

sequential two-step single-electron O_2 reduction (Eqs. (3) and (4)) [6]. However, the photoinduced holes (h^+) of g-C_3N_4 are less active for water oxidation because of the relative low valence band (VB) potential (Eq. (5)) [7]. The relative low h^+ consumption leads to electron-hole recombination, thus limiting the utilization of e^- for O_2 reduction to H_2O_2. To solve the above problem, two approaches have been adopted: 1) quenching the h^+ with the addition of organic electron donor to utilize more e^- for O_2 reduction to H_2O_2 [8]; and 2) positively shifting the VB potential of g-C_3N_4-based catalysts to promote the water oxidation [[5]]. However, the above approaches possess disadvantages: 1) using organic electron donor results in the loss of chemical energy, the introduction of side products, and the increase in cost due to the use of chemicals other than H_2O [5b]; and 2) the positive shifting of the VB potential may generate hydroxyl radical (˙OH) [4d,5e], which can tear the heptazine unit directly from g-C_3N_4 to form cyameluric acid and further release nitrates into the aqueous environment [9]. Therefore, it is highly desired to develop a new strategy of enhancing the h^+ consumption to promote the e^- utilization for O_2 reduction to H_2O_2 and maintaining the chemical stability of g-C_3N_4-based catalysts.

$$H_2O + 2h^+ \rightarrow 1/2O_2 + 2H^+ \ (1.23\ V\ vs.\ NHE) \quad (5)$$

$$^{\cdot}O_2^- + h^+ \rightarrow {}^1O_2\ (0.34\ V\ vs.\ NHE) \quad (6)$$

Since the oxidation of superoxide radicals ($^{\cdot}O_2^-$) to singlet oxygen ($^1O_2$) is thermodynamically favored (0.34 V vs NHE), the $^{\cdot}O_2^-$ can be oxidized by h^+ to $^1O_2$ (Eq. (6)) [10]. Furthermore, it has been proved that the $^1O_2$ can promote the H_2O_2 production in the presence of dissolved organic matter (DOM) as organic electron donors [11]. Negatively shifting the CB potential of g-C_3N_4-based catalysts by incorporating the electrons transfer materials into the g-C_3N_4 framework can enhance the single-electron reduction of O_2 to $^{\cdot}O_2^-$ and further promote the photocatalytic H_2O_2 production [6b,6c]. In addition, g-C_3N_4 is chemical stable towards $^{\cdot}O_2^-$ [9]. Therefore, incorporating the electrons transfer materials into the g-C_3N_4 framework and investigating the $^1O_2$ generation from $^{\cdot}O_2^-$ during the photocatalytic H_2O_2 production over g-C_3N_4-based catalysts is essential for enhancing the h^+ consumption and maintaining the chemical stability of g-C_3N_4-based catalysts. As efficient electrocatalysts for hydrogen evolution reaction (HER) and overall water splitting, the polyoxometalates (POMs)-derived metal oxides are capable of accepting, transporting and storing electrons [12]. Therefore, incorporating the POMs-derived metal oxides into g-C_3N_4 framework can generate more e- for O_2 reduction. Herein, the hybrid catalyst of g-C_3N_4-CoWO has been prepared through the calcination of the g-C_3N_4 precursor of 3-amino 1, 2, 4-triazole (3-AT) and the POMs precursor of $(NH_4)_8Co_2W_{12}O_{42}$ (NH_4-Co_2W_{12}). The hybrid catalyst of g-C_3N_4-CoWO with well-defined and stable structure exhibits efficient catalytic performance (9.7 μmol h^{-1}) for photocatalytic H_2O_2 production in the absence of organic electron donor under visible light. The catalytic and characterization results reveal that the incorporation of CoWO into g-C_3N_4 framework can enhance the single-electron reduction of O_2 to $^{\cdot}O_2^-$ and furthermore promote the $^{\cdot}O_2^-$ oxidation to $^1O_2$ by h^+. The enhanced h^+ consumption and the $^1O_2$ transferred from $^{\cdot}O_2^-$ can promote the photocatalytic H_2O_2 production over g-C_3N_4-CoWO. In addition, the recycle experiment results reveal that the heterogeneous g-C_3N_4-CoWO is catalytic stable.

2. Experimental section

2.1. Chemicals

3-amino 1, 2, 4-triazole (3-AT), melamine, urea, cobalt(II) acetate ($Co(Ac)_2$), ammonium metatungstate ($(NH_4)_6H_2W_{12}O_{40}$), nitro blue tetrazolium (NBT), 1,3-diphenylisobenzofuran (DPBF), *p*-benzoquinone (PBQ), L-Histidine (L-His), ammonium oxalate ($(NH_4)_2C_2O_4$), Rose Bengal (RB), and *tris*(2,2′-bipyridine)ruthenium dichloride ([Ru(bpy)$_3$]Cl_2·$6H_2O$) were purchased from Alfa Asear company and used as received without further purification. MWCNT (purity > 95%) were purchased from Chengdu Organic Chemicals Co. Ltd, Chinese Academy of Sciences. 5,5-dimethyl-1-pyrroline (DMPO), 2,2,6,6-tetramethylpiperidine-1-oxyl (TEMPO) and 2,2,6,6-Tetramethyl-4-piperidone (TEMP) were purchased from Sigma-Aldrich company. $(NH_4)_8Co_2W_{12}O_{42}$ (NH_4-Co_2W_{12}) [13] were synthesized and characterized in accordance with the literature.

2.2. Preparation of g-C_3N_4 [14]

3-AT (6.00 g, 0.07 mol) was placed in a quartz boat and heated under N_2 flow at 550 °C for 4 h at a rate of 3 °C min^{-1}. Then, the quartz boat was cooled to room temperature naturally. The obtained product was collected and ground into fine powder for further use. Based on the EA analysis, the formula of g-C_3N_4 was determined to be $C_{1.68}N_4H_{2.02}O_{1.21}$.

2.3. Preparation of CoWO

NH_4-Co_2W_{12} (6.00 g, 1.91 mmol) was placed in a quartz boat and heated under N_2 flow at 550 °C for 4 h at a rate of 3 °C min^{-1}. Then, the quartz boat was cooled to room temperature naturally. The obtained product was collected and ground into fine powder for further use. Based on the EA and ICP analysis, the formula of CoWO was determined to be $Co_{0.98}W_{6.02}O_{21.06}$.

2.4. Preparation of g-C_3N_4-CoWO

3-AT (4.00 g, 0.05 mol) and NH_4-Co_2W_{12} (2.00 g, 0.67 mmol) were completely mixed in deionized water and kept stirring for 24 h, and then allowed to remove water at 90 °C. Then the precursors were placed in a quartz boat and heated under N_2 flow at 550 °C for 4 h at a rate of 3 °C min^{-1}. Then, the quartz boat was cooled to room temperature naturally. The obtained product was collected and ground into fine powder for further use. Based on the EA and ICP analysis, the formula of g-C_3N_4-CoWO was determined to be $C_{1.67}N_4H_{2.01}Co_{0.06}W_{0.37}O_{2.47}$. For comparison, g-$C_3N_4$-Co and g-$C_3N_4$-WO have been prepared through the same method with the same molar of Co ($Co(Ac)_2$ as precursor) or W ($(NH_4)_6H_2W_{12}O_{40}$ as precursor) as g-C_3N_4-CoWO. Based on the EA and ICP analysis, the formula of g-C_3N_4-Co and g-C_3N_4-WO were determined to be $C_{1.67}N_4H_{2.01}Co_{0.06}O_{1.29}$ and $C_{1.67}N_4H_{2.01}W_{0.37}O_{2.43}$, respectively. To investigate the effect of precursor, g-C_3N_4-CoWO-Melamine has been prepared through the same method using melamine to instead 3-AT. Based on the EA and ICP analysis, the formula of g-C_3N_4-CoWO-Melamine were determined to be $C_{2.30}N_4H_{1.96}Co_{0.06}W_{0.37}O_{2.47}$.

2.5. Photocatalytic hydrogen peroxide production

The photocatalytic activities were evaluated by the activation of oxygen under light irradiation (λ ≥ 420 nm). A 300 W Xenon lamp (Perfect Light Company, Beijing) was chosen as light source. During each photocatalytic performance, 0.10 g of catalyst was dispersed into 100 ml of water in a container (1 g L^{-1} catalyst). After that, the dispersion was stirred in the dark for 60 min to ensure the adsorption-desorption equilibrium among the catalyst, dissolved oxygen and water before light irradiation. During the irradiation, 1.50 ml of the suspensions was taken from the reaction cell at given time intervals, and then filtrated to remove the catalysts. The concentrations of H_2O_2 generated were determined by iodometric titration [15]. After completion of the reaction, the catalysts can be recovered by centrifugation, washed with water, and dried at 60 °C in air. To investigate the decomposition behavior of H_2O_2 over the photocatalysts, a catalyst of 1 g L^{-1} was dispersed in H_2O_2 solution (initial concentration: 1 mM) and irradiated for 60 min under continuous stirring.

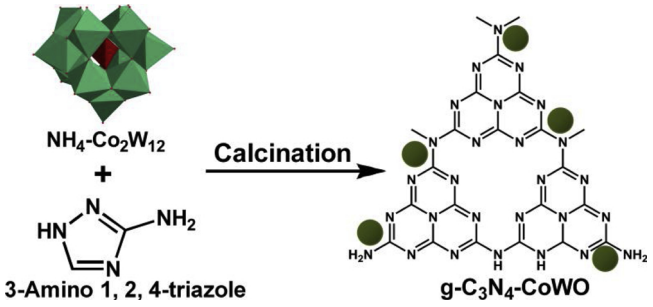

Fig. 1. Preparation process of g-C_3N_4-CoWO.

3. Results and discussion

3.1. Preparation of g-C_3N_4-CoWO

As shown in Fig. 1, the hybrid catalyst of g-C_3N_4-CoWO has been prepared through the calcination of the g-C_3N_4 precursor of 3-AT and the POMs precursor of NH_4-Co_2W_{12}. The XRD patterns of NH_4-Co_2W_{12}, CoWO, g-C_3N_4, g-C_3N_4-Co, g-C_3N_4-WO and g-C_3N_4-CoWO are shown in Fig. S1A. The NH_4-Co_2W_{12} possesses the typical peaks of $[Co_2W_{12}O_{40}]^{8-}$ cluster [13]. The NH_4-Co_2W_{12} has been completely transformed to the $CoWO_4$ (JCPDS 15-0867) phase after calcination [16]. The g-C_3N_4 has two distinct diffraction peaks at 13.1° and 27.6°, which correspond to the graphitic materials as the (100) and (002) diffraction planes in JCPDS 87–1526 [17]. For g-C_3N_4-CoWO, the peaks intensities at 13.0° and 27.5° decreases compared with g-C_3N_4 (Fig. S1A), which indicates that the polymeric structure of g-C_3N_4-CoWO is possibly derived from the simultaneous condensation of melamine and NH_4-Co_2W_{12}. In the case of 3-AT (Fig. S1B), melamine-based products are dominant at 350 °C, but *tri*-s-triazine (melem) starts to generate as a result of melamine rearrangement over 350 °C [18]. With a further increase in the temperature, the condensation of melem to poly-meric networks induces the formation of g-C_3N_4 at around 550 °C. For NH_4-Co_2W_{12} (Fig. S1C), the structure of $[Co_2W_{12}O_{40}]^{8-}$ cluster remains untouched at 350 °C, but transforms to the $CoWO_4$ phase at about 550 °C. The XRD pattern of 3-AT and NH_4-Co_2W_{12} mixture (the same molar ratio as the preparation of g-C_3N_4-CoWO) reveals that the melamine and $CoWO_4$ phase peaks disappear with an increase in the calcination temperature (Fig. S1D), and trace peaks of melamine and CoWO are no longer observed. The above results reveal that the CoWO has been well incorporated into the g-C_3N_4 framework without leaving melamine or CoWO unreacted [8b]. Fig. S2 shows the IR spectra of NH_4-Co_2W_{12}, CoWO, g-C_3N_4, g-C_3N_4-Co, g-C_3N_4-WO and g-C_3N_4-CoWO. The peaks in the range of 1150-1825 cm^{-1} have been observed in g-C_3N_4, g-C_3N_4-Co, g-C_3N_4-WO and g-C_3N_4-CoWO, which are the typical vibrations of heptazine-based molecular units [19]. The vibrations from 523 to 968 cm^{-1} corresponding to the chemical bonds of CoWO can be found in both CoWO and g-C_3N_4-CoWO [12]. The above IR results indicate that the structure of g-C_3N_4 and CoWO has been well preserved after incorporation. Thermogravimetry analysis (TGA) curves for g-C_3N_4, CoWO and g-C_3N_4-CoWO in air are shown in Fig. S3. The total weight loss of g-C_3N_4 is 98.59% between 30 and 708 °C due to the direct thermal decomposition of g-C_3N_4. For CoWO, the weight loss in the range of 30–223 °C range (3.96%) corresponds to the loss of physisorbed water. In the case of g-C_3N_4-CoWO, the weight loss in the range of 30–704 °C range (51.28%) is mainly due to the thermal decomposition of g-C_3N_4. The TGA result of CoWO confirms that no lattice oxygen has stripped out of CoWO during the preparation of g-C_3N_4-CoWO, and the TGA result of g-C_3N_4-CoWO reveals that the weight percentage of CoWO for g-C_3N_4-CoWO is about 48.72%. The nitrogen adsorption-desorption isotherms and pore size distribution patterns for CoWO, g-C_3N_4, g-C_3N_4-Co, g-C_3N_4-WO and g-C_3N_4-CoWO are shown in Fig. S4. The isotherms for g-C_3N_4, g-C_3N_4-Co, g-C_3N_4-WO and g-C_3N_4-CoWO (Fig. S4A) show type IV isotherm with a type H3 hysteresis loop. These catalysts present one peak centered at 3.5 nm in a broad pore-size distribution curve (1–100 nm) in Fig. S4B [20]. As listed in Table S1, the higher surface area of g-C_3N_4-CoWO (24.2 m^2/g) than that of g-C_3N_4 (6.5 m^2/g) reflects a large number of active sites and are thus beneficial for the photocatalytic H_2O_2 production [21]. Furthermore, O_2 temperature programmed desorption (O_2-TPD) has been performed to detect the changes of oxygen species after incorporation (Fig. S5). The TGA results for CoWO, g-C_3N_4 and g-C_3N_4-CoWO in air reveal that the above catalysts are stable in air below 530 °C (Fig. S3). In O_2-TPD profiles, the signals recorded below 700 °C are generally denoted as α-oxygen species and correspond to oxygen species adsorbed on the surface oxygen vacancies, whereas those recorded above 700 °C are known as β-oxygen species related to lattice oxygen, which causes generation of oxygen vacancies and reduced cations. Generally, the amount of α-O_2 can be considered as a measure of the oxygen vacancies, while the amount as well as the onset temperature of β-O_2 desorbed reflects the lattice oxygen mobility [22]. Along with the O_2-TPD curves, it is clearly confirmed that the oxygen desorption peaks of CoWO, g-C_3N_4 and g-C_3N_4-CoWO are mainly attributed to the adsorbed O_2. The g-C_3N_4-CoWO exhibits a stronger O_2-TPD signal than CoWO, g-C_3N_4, indicating that the g-C_3N_4-CoWO possesses a strong ability for O_2 adsorption [23]. The above results reveal that the incorporation of CoWO into g-C_3N_4 framework can enhance the O_2 adsorption ability of CoWO. Fig. S6 shows the zeta potential values of g-C_3N_4 (-15.6 mV), g-C_3N_4-CoWO (-42.1 mV) and CoWO (-54.3 mV) are all negative in water, indicating that the surfaces of these catalysts are negatively charged. It is highly possible that the incorporation of CoWO into g-C_3N_4 framework has greatly changed the surface property of g-C_3N_4 as observed in the decreasing of zeta potential. The g-C_3N_4-CoWO with more negative charge can react with H^+ more easily than g-C_3N_4, and thus promote the photocatalytic H_2O_2 production [15,24]. Combining the EA and ICP analysis in Table S2, the molecular formulas of g-C_3N_4, g-C_3N_4-Co, g-C_3N_4-WO and g-C_3N_4-CoWO can be given as $C_{1.68}N_4H_{2.02}O_{1.21}$, $C_{1.67}N_4H_{2.01}Co_{0.06}O_{1.29}$, $C_{1.67}N_4H_{2.01}W_{0.37}O_{2.43}$ and $C_{1.67}N_4H_{2.01}Co_{0.06}W_{0.37}O_{2.47}$ (47.62 wt% CoWO).

Fig. 2 shows the C 1 s, N 1 s, Co 2p, W 4f and O 1 s XPS spectra of CoWO, g-C_3N_4 and g-C_3N_4-CoWO. As shown in Fig. 2A, XPS peaks of C 1 s for g-C_3N_4 and g-C_3N_4-CoWO can be fitted with three peaks at binding energies of around 283.3, 284.4 and 287.5 eV, which are ascribed to the tertiary carbon C-N_3 groups, the C-NH_2 groups and the C—C groups, respectively [14]. Nevertheless, the XPS peaks of N 1 s (Fig. 2B) for g-C_3N_4 can be fitted with three peaks at 398.0, 399.6, and 404.2 eV, which are assigned to the N-(C_2), N-(C_3), and -NH_2, respectively [4b]. The C 1s and N1s XPS results reveal that the primary structure of g-C_3N_4 has been well preserved after incorporation. As shown in Fig. 2C, the asymmetrical Co $2p_{3/2}$ XPS spectra of CoWO and g-C_3N_4-CoWO can be decomposed into two components at binding energies of 780.1 and 781.9 eV, which correspond to surface Co^{3+} and Co^{2+} species, respectively [25]. The surface Co^{3+}/Co^{2+} molar ratio decreases in the following order: g-C_3N_4-CoWO (2.77) > CoWO (1.27). The surface Co^{3+}/Co^{2+} molar ratio is consistent with the catalytic performance because the Co^{3+}/Co^{2+} recycle can supply the electrons for oxygen reduction [3a]. In addition, XPS peaks of W 4f (Fig. 2D) for CoWO and

g-C_3N_4-CoWO can be fitted with two peaks at binding energies of around 34.9 and 37.1 eV (W $4f_{7/2}$ and W $4f_{5/2}$), which are consistent with a W(VI) oxidation state [12]. The Co 2p and W 4f XPS results reveal that the primary structure of CoWO has been well preserved after incorporation. The results in Fig. 2E indicate that O 1s exhibits signals at binding energies of 529.9 and 531.1 eV, which correspond to surface lattice oxygen (O_{latt}) species and surface adsorbed oxygen (O_{ads}) [26]. The surface O_{ads}/O_{latt} molar ratio decreases in the following order: g-C_3N_4-CoWO (1.11) > CoWO (0.79) > g-C_3N_4 (0.33). The XPS O 1 s results are consistent with the above O_2-TPD results, which reveal that the incorporation of CoWO into g-C_3N_4 framework can enhance the O_2

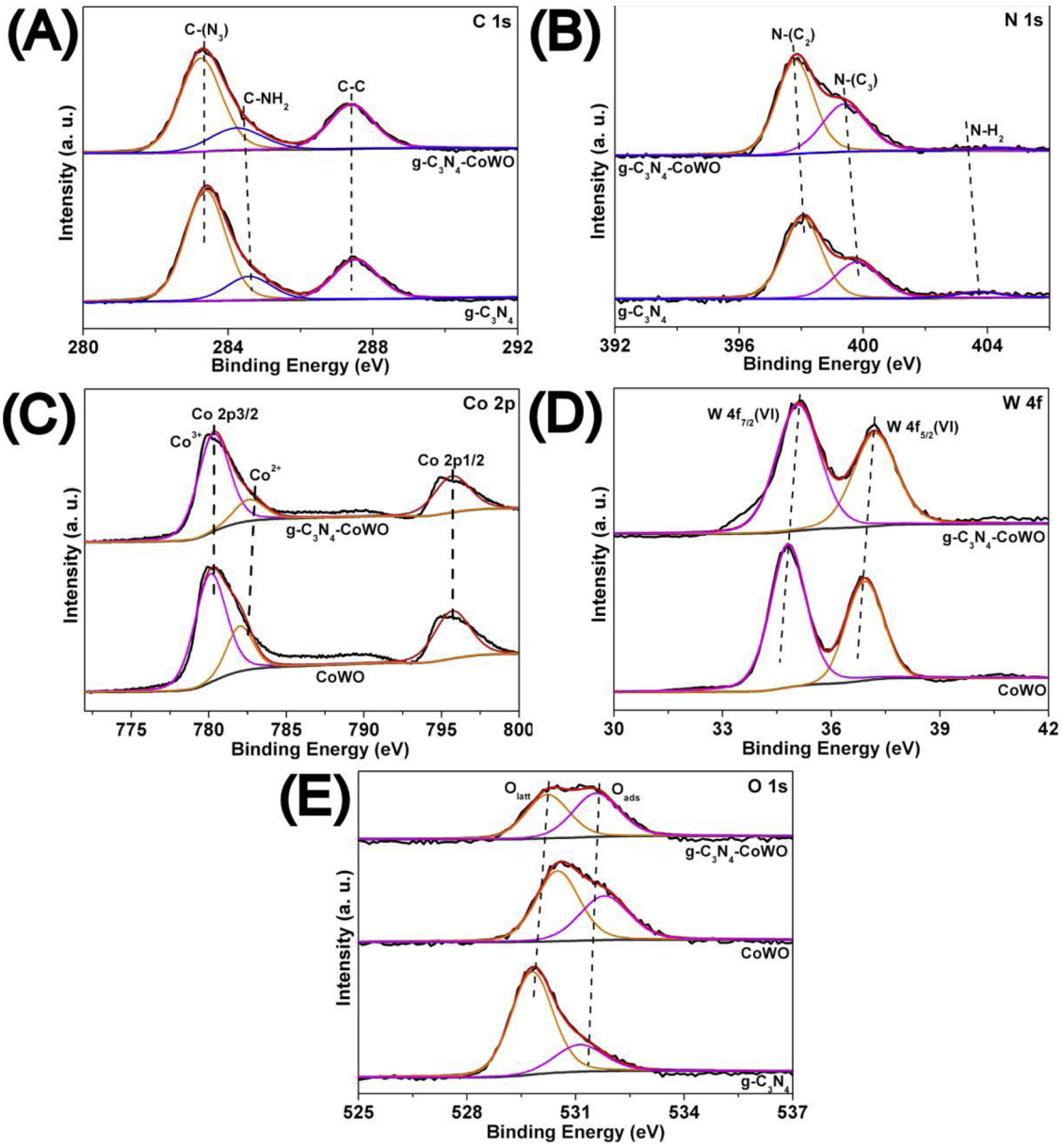

Fig. 2. C 1s (A), N 1s (B), Co 2p (C), W 4f (D) and O 1s (E) XPS spectra of g-C_3N_4, CoWO and g-C_3N_4-CoWO.

adsorption ability of CoWO. The above XPS results reveal that the CoWO has been incorporated into g-C_3N_4 framework and the primary structure of g-C_3N_4 and CoWO has been well preserved after incorporation. Furthermore, the incorporation of CoWO into g-C_3N_4 framework can enhance the O_2 adsorption ability of CoWO.

Fig. 3 and S9-S11 are the TEM images of g-C_3N_4, g-C_3N_4-Co, g-C_3N_4-WO and g-C_3N_4-CoWO, which exhibit sheet-like structure [27]. As shown in Fig. 3D, it is clear that the crystalline CoWO are well incorporated into the g-C_3N_4 framework [12]. To investigate the incorporation of CoWO into g-C_3N_4 framework, STEM-Mapping characterization has been performed. As shown in Fig. S14A and B, g-C_3N_4-CoWO remains the sheet-like structure after incorporation. The elemental mappings of C, N, Co, W and O (Fig. S14C-H) clearly exhibit the CoWO are well incorporated into the g-C_3N_4 framework [8b].

The above characterization results confirm that the CoWO has been incorporated into g-C_3N_4 framework to form the hybrid catalyst of g-C_3N_4-CoWO. Furthermore, the catalytic performance of g-C_3N_4-CoWO should be investigated.

3.2. Catalytic performance of g-C_3N_4-CoWO

The photocatalytic H_2O_2 production over different catalysts has been conducted and monitored in an O_2-equilibrated conditions and light irradiation ($\lambda \geq 420$ nm) in the absence of organic electron donor at 25 °C. As shown in Fig. 4A, the H_2O_2 can be rapidly generated over g-C_3N_4-CoWO and the amounts of formed H_2O_2 can reach 18.7 μmol in 60 min. For comparison, g-C_3N_4-WO and g-C_3N_4-Co have been prepared through the same method with the same molar of Co ($Co(Ac)_2$ as precursor) or W ($(NH_4)_6H_2W_{12}O_{40}$ as precursor) as g-C_3N_4-CoWO. The g-C_3N_4-WO (6.9 μmol in 60 min) and g-C_3N_4-Co (1.4 μmol in 60 min) show lower catalytic performance than g-C_3N_4-CoWO (18.7 μmol in 60 min). The g-C_3N_4-CoWO-IMP through the impregnation method with the same CoWO weight percentage as g-C_3N_4-CoWO also shows lower catalytic performance (< 0.1 μmol in 60 min). The catalytic performance of individual g-C_3N_4 (< 0.1 μmol in 60 min) or CoWO (< 0.1 μmol in 60 min) is lower than that of g-C_3N_4-CoWO (18.7 μmol in 60 min). The reaction cannot proceed in the absence of catalyst (< 0.1 μmol in 60 min). The above results reveal that the catalytic

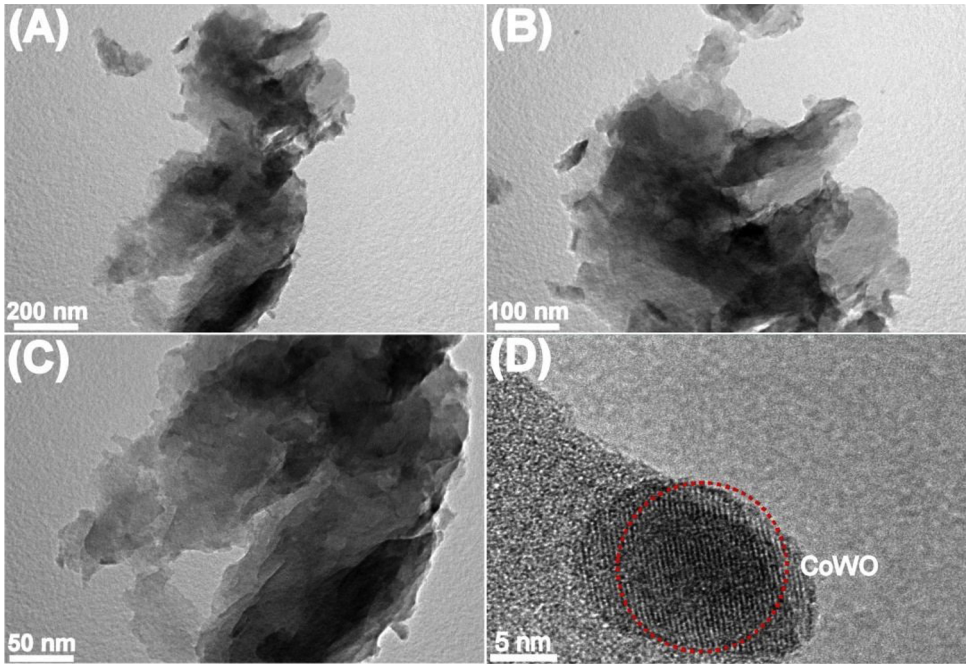

Fig. 3. TEM images (A–D) of g-C_3N_4-CoWO.

performance of g-C_3N_4-CoWO (18.7 μmol in 60 min) is much higher than that of g-C_3N_4-CoWO-IMP (< 0.1 μmol in 60 min). As shown in Fig. S15, the XRD pattern of g-C_3N_4-CoWO-IMP shows the typical peaks of both g-C_3N_4 and CoWO while the XRD pattern of g-C_3N_4-CoWO only show the peaks of g-C_3N_4. The XRD result indicates that the CoWO disperses on the surface of g-C_3N_4 in the g-C_3N_4-CoWO-IMP and the CoWO has been well incorporated into the g-C_3N_4 framework without leaving melamine or CoWO unreacted in the g-C_3N_4-CoWO. The incorporation of CoWO into the g-C_3N_4 framework can enhance the O_2 adsorption ability [23] and facilitate the interfacial electrons transfer to O_2 [8b], which can promote the catalytic performance for photocatalytic H_2O_2 production. Fig. S16A shows that the g-C_3N_4-CoWO exhibits better catalytic performance (18.7 μmol in 60 min) for the photocatalytic H_2O_2 production than g-C_3N_4-CoWO-Melamine using melamine to instead 3-AT (7.1 μmol in 60 min). The CO_2-TPD (Fig. S16B) and EA (Table S2) results reveal that the g-C_3N_4-CoWO using 3-AT as precursor can generate more carbon vancies (-NH_2 groups) than g-C_3N_4-CoWO-Melamine using melamine as precursor [4b,14]. The carbon vacancies can enhance the O_2 adsorption ability [23] and facilitate the interfacial electrons transfer to O_2 [8b], which can promote the catalytic performance for photocatalytic H_2O_2 production. The photocatalytic H_2O_2 production over g-C_3N_4-WO and g-C_3N_4-CoWO has been performed under N_2- and O_2-equilibrated conditions to investigate the role of O_2 in the photocatalytic H_2O_2 production (Fig. S17 A). Generally, the photoexcited conduction band (CB) electrons can be scavenged by dissolved O_2 under O_2-equilibrated conditions but the protons should uptake the electrons in the absence of O_2 (N_2-equilibrated conditions) [8b]. Under N_2-equilibrated conditions, no H_2O_2 can be formed over both g-C_3N_4-WO and g-C_3N_4-CoWO, confirming that the H_2O_2 is generated through the O_2 reduction. Fig. S17B

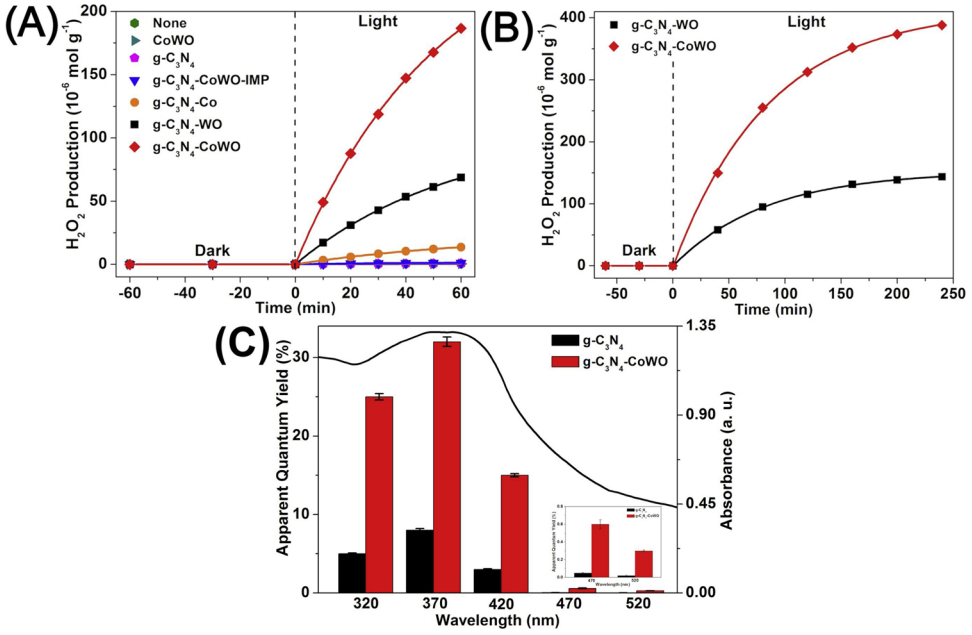

Fig. 4. Photocatalytic H_2O_2 formation over different catalysts in 60 min (A). Reaction conditions: water (100 ml), catalyst (0.10 g, 1 g L^{-1}), O_2-equilibrated, λ ≥ 420 nm, 25 °C. Photocatalytic H_2O_2 formation over g-C_3N_4-WO and g-C_3N_4-CoWO in 240 min (B). Reaction conditions: water (100 ml), catalyst (0.10 g, 1 g L^{-1}), O_2-equilibrated, λ ≥ 420 nm, 25 °C. Apparent quantum yield (AQY) of g-C_3N_4 and g-C_3N_4-CoWO for photocatalytic H_2O_2 production at selected wavelengths (C). Reaction conditions: water (100 ml), g-C_3N_4 or g-C_3N_4-CoWO (0.10 g, 1 g L^{-1}), O_2-equilibrated, 25 °C.

show that under N_2-equilibrated conditions the H_2 can be detected g-C_3N_4-WO (15.3 μmol in 60 min) and g-C_3N_4-CoWO (34.1 μmol in 60 min) while under O_2-equilibrated conditions the H_2 cannot be detected over g-C_3N_4-WO (< 0.1 μmol in 60 min) and g-C_3N_4-CoWO (< 0.1 μmol in 60 min). Under N_2-equilibrated conditions the e^- of the CB possess the ability for hydrogen evolution reaction while under O_2-equilibrated conditions the e^- of the CB are utilized for the O_2 reduction reaction [28].

$$[H_2O_2] = \frac{K_f}{K_d}(1 - e^{K_d t}) \quad (7)$$

The formation and decomposition of H_2O_2 over catalysts proceeds through two competitive pathways owing to the thermodynamic instability of H_2O_2 at room temperature [29]. The K_f and K_d values have been estimated by fitting the data in Fig. 4A according to Eq. (7) and the results are presented in Table S3 [30]. In order to investigate the stability of different catalysts, the reaction time has been extended to 240 min. The maximum amounts of formed H_2O_2 over g-C_3N_4-CoWO and g-C_3N_4-WO can be obtained as 38.8 and 14.4 μmol in 240 min, respectively (Fig. 4B), which gives the H_2O_2 formation rate of 9.7 and 3.6 μmol h^{-1} for g-C_3N_4-CoWO and g-C_3N_4-WO (Table S3). The values of K_f obtained from the photocatalytic H_2O_2 production over different catalysts decrease in the following order: g-C_3N_4-CoWO (5.2711 μmol min^{-1}) > g-C_3N_4-WO (1.7709 μmol min^{-1}) > g-C_3N_4-Co (0.3444 μmol min^{-1}) > g-C_3N_4-CoWO-IMP (0.0453 μmol min^{-1}) > g-C_3N_4 (0.0313 μmol min^{-1}) > CoWO (0.0222 μmol min^{-1}) > None (0.0109 μmol min^{-1}), which is consistent with the above H_2O_2 formation rate of different catalysts (Fig. 4A).

$$-\frac{dc_t}{dt} = k_0 \quad (8)$$

The photocatalytic H_2O_2 decomposition over different catalysts has been conducted with an initial H_2O_2 concentration of 1 mM to investigate the decomposition behavior of H_2O_2 in the presence of catalysts. As shown in Fig. S18A, the H_2O_2 decomposes activity of g-C_3N_4-CoWO (75% in 60 min) is higher than those of g-C_3N_4-WO (61% in 60 min), g-C_3N_4-Co (15% in 60 min), g-C_3N_4-CoWO-IMP (9% in 60 min), g-C_3N_4 (6% in 60 min), CoWO (15%) and None (6% in 60 min). Two reasons can be presented for the results that the photocatalytic H_2O_2 production of g-C_3N_4-CoWO is higher than that of g-C_3N_4-WO: 1) the incorporation of CoWO into g-C_3N_4 framework can introduce more negative surface charge as observed in the decreasing of zeta potential from -36.4 mV (g-C_3N_4-WO) to -42.1 mV (g-C_3N_4-CoWO). More negative charge can react with H^+ more easily and thus promote the photocatalytic H_2O_2 production [15,24]; and 2) the incorporation of CoWO into g-C_3N_4 framework can enhance the O_2 adsorption ability [23] and facilitate the interfacial electrons transfer to O_2 [8b].

Since the POMs precursors are $(NH_4)_6H_2W_{12}O_{40}$ and $(NH_4)_8Co_2W_{12}O_{42}$, the catalysts of g-C_3N_4-WO and g-C_3N_4-CoWO may contain NH_3 residues that can act as the electron donor for the photocatalytic H_2O_2 production. To remove the possible existing NH_3 residues, the catalysts of g-C_3N_4-WO and g-C_3N_4-CoWO have been dispersed in water after calcination and the suspensions keep stirring for 24 h to prepare the catalysts of g-C_3N_4-WO/H_2O and g-C_3N_4-CoWO/H_2O. The photocatalytic H_2O_2 production over g-C_3N_4-WO/H_2O, g-C_3N_4-CoWO/H_2O g-C_3N_4-WO and g-C_3N_4-CoWO has been performed (Fig. S19). The results reveal that the catalytic performance of g-C_3N_4-WO and g-C_3N_4-CoWO remain unchanged after stirring in water for 24 h and rule out the existence of NH_3 residues in catalysts of g-C_3N_4-WO and g-C_3N_4-CoWO.

It should be noted that under similar reaction conditions over the g-C_3N_4-based catalysts in the absence of organic electron donors, the H_2O_2 formation rate (9.7 μmol h^{-1}) over g-C_3N_4-CoWO is more than those over g-C_3N_4-BDI_{50} (0.5 μmol h^{-1}) [5a], g-C_3N_4-PDI_{51} (1.0 μmol h^{-1}) [7], g-C_3N_4-PDI_{51}-rGOs (1.2 μmol h^{-1}) [4a], g-C_3N_4-NiFeO (1.8 μmol h^{-1}) [5b], 3DOM g-C_3N_4-PW_{11} (2.4 μmol h^{-1}) [5c], g-C_3N_4-PWO (2.9 μmol h^{-1}) [6c], oxygen-enriched g-C_3N_4 (5.4 μmol h^{-1}) [5d] and Cv-g-C_3N_4 (9.2 μmol h^{-1}) [4b]. Nevertheless, the H_2O_2 formation rate (9.7 μmol h^{-1}) over g-C_3N_4-CoWO is more than those over TiO_2-CoPi-rGOs (2.3 μmol h^{-1}) [3a] and CdS-$rGOs_{20}$ (0.5 μmol h^{-1}) [3d].

The apparent quantum yields (AQY) of photocatalytic H_2O_2 production have been compared between g-C_3N_4 and g-C_3N_4-CoWO. Fig. 4C shows that the AQY of g-C_3N_4-CoWO in the UV range is 24.8% at 320 nm and 32.2% at 370 nm. In the visible light region, AQY at 420 nm is 15.1%, which is 5 times higher than that for g-C_3N_4 at 420 nm (Φ_{420} = 2.9%). Under similar reaction conditions over the g-C_3N_4-based catalysts, the AQY value at 420 nm for g-C_3N_4-CoWO (Φ_{420} = 15.1%) is higher than those for g-C_3N_4-PDI_{51} (Φ_{420} = 2.7%) [[27]], g-C_3N_4-BDI_{50} (Φ_{420} = 4.8%) [5a], g-C_3N_4-PDI_{51}-rGOs (Φ_{420} = 6.0%) [4a], g-C_3N_4-SiW_{11} (Φ_{420} = 6.5%) [27b], g-C_3N_4-KPO (Φ_{420} = 8.1%) [8b], oxygen-enriched g-C_3N_4 (Φ_{420} = 10.2%) [5d] and holey defective g-C_3N_4 (Φ_{420} = 11.5%) [8d], but inferior to that for g-C_3N_4-KPF_6 (Φ_{420} = 24.3%) [8e].

The oxygen evolution reaction (OER) and photocatalytic O_2 evolution results in Fig. S20 suggest that the g-C_3N_4-CoWO can act as a catalyst for water oxidation [5b,5c]. Therefore, the relative high H_2O_2 formation rate and AQY value at 420 nm among the reported catalysts make g-C_3N_4-CoWO a promising catalyst for photocatalytic H_2O_2 production in the absence of organic electron donors.

3.3. Structure-catalytic performance relationship of g-C_3N_4-CoWO

Photoelectrochemical characterization should be performed to clarify the reason for the efficient catalytic activity of g-C_3N_4-CoWO. As shown in Fig. S21A, the photo-current densities of the g-C_3N_4-based catalysts decrease in the following order: g-C_3N_4-CoWO (0.57 μA cm^{-2}) > g-C_3N_4-WO (0.33 μA cm^{-2}) > g-C_3N_4-Co (0.13 μA·cm^{-2}) > g-C_3N_4 (0.05 μA cm^{-2}). Photoelectrochemical impedance spectroscopy (EIS) results are shown in Fig. S21B. The diameters of Nyquist semicircle for the g-C_3N_4-based catalysts increase in the following order: g-C_3N_4-CoWO < g-C_3N_4-WO < g-C_3N_4-Co < g-C_3N_4. The emission peak appearing at about 543 nm in photoluminescence (PL) spectra of the g-C_3N_4-based catalysts is attributed to the direct electron-hole recombination of band transition. Compared with g-C_3N_4, g-C_3N_4-CoWO possess a much weaker emission peak (Fig. S22A). The above results reveal that the incorporation of CoWO into g-C_3N_4 framework can enhance the charge separation of g-C_3N_4-CoWO.

Electrochemical rotating disk electrode (RDE) analysis of oxygen reduction reaction (ORR) further investigates the electrons transfer of O_2 reduction. Fig. S23

shows the LSV curves of g-C_3N_4, g-C_3N_4-Co, g-C_3N_4-WO and g-C_3N_4-CoWO measured on RDE in an O_2-saturated 0.1 M phosphate buffer solution (pH 7) at different rotating speeds. Fig. 5A summarizes the Koutecky-Levich plots of the data at -0.9 V vs. Ag/AgCl [31]. The n values for the g-C_3N_4-based catalysts decrease in the following order: g-C_3N_4-CoWO (n = 1.95) > g-C_3N_4-WO (n = 1.73) > g-C_3N_4-Co (n = 1.36) > g-C_3N_4 (n = 1.18), suggesting that the CoWO combined with g-C_3N_4 can promote the electrons generation. The rotating ring disc electrode (RRDE) of oxygen reduction reaction (ORR) results in Fig. S24-S28 show the values of transferred electron during the ORR decrease in the following order: g-C_3N_4-CoWO (n = 1.95) > g-C_3N_4-WO (n = 1.73) > g-C_3N_4-Co (n = 1.36) > g-C_3N_4 (n = 1.18), which is consisted with the above ORR-RDE results. Furthermore, the ORR-RRDE results reveal that the g-C_3N_4-Urea with urea as precursor shows the value of transferred electron during the ORR is 1.68 (Fig. S29). The value of transferred electron during the ORR for the g-C_3N_4 with 3-amino 1, 2, 4-triazole (n = 1.18) as precursor is quite different from that for g-C_3N_4-Urea with urea as precursor (n = 1.68) because of the different precursors. In order to investigate the generation of photo-induced electrons (e^-), electron spin resonance (ESR) analysis with 2,2,6,6-tetramethylpiperidine-1-oxyl (TEMPO) as a spin-trapping reagent has been performed over the g-C_3N_4-based catalysts. The

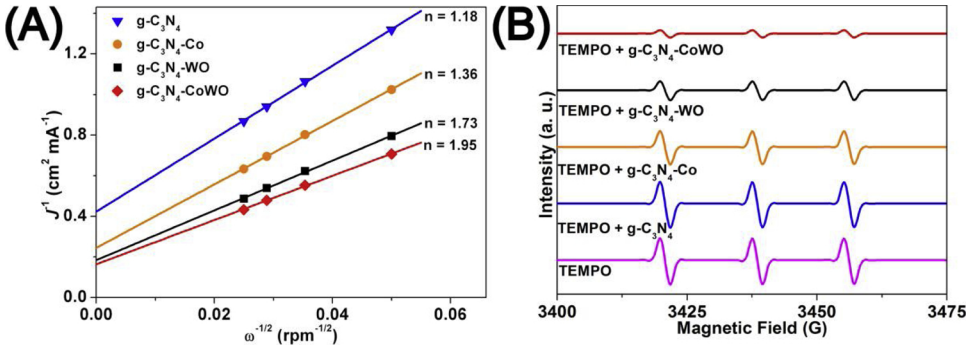

Fig. 5. Koutecky-Levich plots of the ORR data measured by RDE analysis for g-C_3N_4, g-C_3N_4-Co, g-C_3N_4-WO and g-C_3N_4-CoWO (Fig. S23) in a buffered solution (pH 7) at a constant potential of -0.9 V vs Ag/AgCl (A); TEMPO spin trapping ESR technique to investigate the generation of photoinduced electrons during the photoreaction over g-C_3N_4, g-C_3N_4-Co, g-C_3N_4-WO and g-C_3N_4-CoWO (B).

reduction of TEMPO by electrons produces an ESR silent molecule, TEMPOH, and leads to the reduction of intensity and flatting of ESR spectra [32]. As shown in Fig. 5B, when irradiated for 3 min, all the g-C_3N_4-based catalysts cause the reduction of the TEMPO signal, suggesting the electrons transfer from photoexcited the catalysts to TEMPO. The consumption of TEMPO demonstrates that reactive electrons are generated during photo-excitation of the g-C_3N_4-based catalysts. The reduction of TEMPO signal intensity caused by g-C_3N_4-CoWO is much greater than that by g-C_3N_4, indicating that higher reducing ability of photoexcited g-C_3N_4-CoWO than g-C_3N_4. The above results reveal that the CoWO incorporated into g-C_3N_4 framework can promote the e^- generation.

The $^{\cdot}O_2^-$ concentration has been quantified to investigate the role of the $^{\cdot}O_2^-$ in the photocatalytic H_2O_2 production. Nitro **blue** tetrazolium (NBT) has been chosen as a $^{\cdot}O_2^-$ scavenger because NBT can be reduced by $^{\cdot}O_2^-$ and formed **purple** formazan, which is insoluble in water [33]. Fig. 6A and B show the evolution of NBT disappearance and the subsequent formation of $^{\cdot}O_2^-$ during the photocatalytic H_2O_2 production of different catalysts: 1) only the g-C_3N_4-Co, g-C_3N_4-WO and g-C_3N_4-CoWO produce the $^{\cdot}O_2^-$ during the photocatalytic H_2O_2 production; 2) g-C_3N_4-CoWO produce the most $^{\cdot}O_2^-$ among them. To investigate the role of the $^{\cdot}O_2^-$ in the photocatalytic H_2O_2 production, the scavenger experiments using *p*-benzoquinone (PBQ) over g-C_3N_4-WO (Fig. S30A) and g-C_3N_4-CoWO (Fig. 6C) have been performed: the amounts of the formed H_2O_2 gradually decrease with the increase of the PBQ concentration in the reaction system. It should be noted that no H_2O_2 has formed over g-C_3N_4-WO (Fig. S30A) and g-C_3N_4-CoWO (Fig. 6C) when the PBQ concentration reaches 0.40 mM. The above results reveal that no H_2O_2 can form when the two-step single-electron O_2 reduction reaction has been quenched, and rule out the existence of one-step two-electron O_2 reduction reaction over g-C_3N_4-WO and g-C_3N_4-CoWO. ESR analysis with 5,5-dimethyl-1-pyrroline N-oxide (DMPO) as a spin-trapping reagent has been performed to confirm the role of the $^{\cdot}O_2^-$ in the photocatalytic H_2O_2 production [8a]. Fig. 6D reveal that the signal intensity for the solution obtained by photoreaction over g-C_3N_4-CoWO gradually decreases with the addition of PBQ. The g-C_3N_4-WO has the same trend (Fig. S30B). The $^{\cdot}O_2^-$ quantitative and scavenger experiments results combined with the ESR results reveal that: 1) the $^{\cdot}O_2^-$ is involved in the photocatalytic H_2O_2 production over g-C_3N_4-WO and g-C_3N_4-CoWO [6b,6c,34]; and 2) the incorporation of CoWO into the g-C_3N_4 framework can enhance the $^{\cdot}O_2^-$ formation through the single-electron O_2 reduction.

To investigate the role of $^1O_2$ in the photocatalytic H_2O_2 production, the scavenger experiments using L-Histidine (L-His) over g-C_3N_4-WO (Fig. S31A) and g-C_3N_4-CoWO (Fig. 7A) have been performed: the amounts of the formed H_2O_2 gradually decrease with the increase of the L-His concentration in the reaction system. ESR analysis with 2,2,6,6-Tetramethyl-4-piperidone (TEMP) as a spin-trapping reagent has been performed to confirm the role of $^1O_2$ in the photocatalytic H_2O_2 production [10b]. Fig. 7B reveal that the signal intensity for the solution obtained by photoreaction over g-C_3N_4-CoWO gradually decreases with the addition of L-His. The g-C_3N_4-WO has the same trend (Fig. S31B). The $^{\cdot}O_2^-$ concentration over g-C_3N_4-WO (Fig. S31C) and g-C_3N_4-CoWO (Fig. 7C) have been quantified with the addition of L-His: the $^{\cdot}O_2^-$

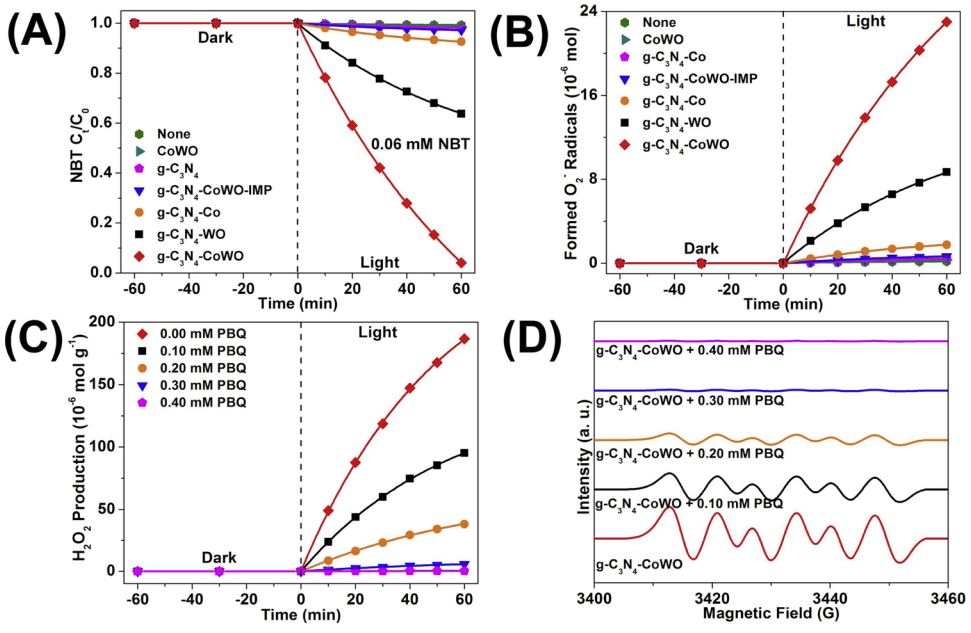

Fig. 6. NBT decomposition during the photoreaction over different catalysts (A) and the $^{\cdot}O_2^-$ formation during the photoreaction over different catalysts (B). Reaction conditions: water (100 ml), catalyst (0.10 g, 1 g L^{-1}), NBT (0.06 mM), O_2-equilibrated, $\lambda \geq 420$ nm, 25 °C. The effect of PBQ on the photocatalytic H_2O_2 production over g-C_3N_4-CoWO (C). Reaction conditions: water (100 ml), g-C_3N_4-CoWO (0.10 g, 1 g L^{-1}), PBQ (0.10, 0.20, 0.30 and 0.40 mM), O_2-equilibrated, $\lambda \geq 420$ nm, 25 °C. DMPO spin trapping ESR technique to measure $^{\cdot}O_2$- generated photoreaction with the addition of PBQ over g-C_3N_4-CoWO (D).

concentrations over g-C_3N_4-WO and g-C_3N_4-CoWO remain unchanged with the increase of the L-His concentration in the reaction system. ESR analysis with DMPO as a spin-trapping reagent has been performed to confirm the $^{\cdot}O_2^-$ concentration with the addition of L-His [8a]. Fig. 7D reveal that the signal intensity for the solution obtained by photoreaction over g-C_3N_4-CoWO remains unchanged with the addition of L-His. The g-C_3N_4-WO has the same trend (Fig. S31D). ESR analysis with TEMP as a spin-trapping reagent has been performed to investigate the role of $^{\cdot}O_2^-$ in the formation of $^1O_2$ [10b]. Fig. 7E reveal that the signal intensity for the solution obtained by photoreaction over g-C_3N_4-CoWO gradually decreases with the addition of PBQ. The g-C_3N_4-WO has the same trend (Fig. S31E). The L-His scavenger experiments and $^{\cdot}O_2^-$ quantitative experiments results combined with the ESR results reveal that: 1) the $^1O_2$ is involved in the photocatalytic H_2O_2 production over g-C_3N_4-WO and g-C_3N_4-CoWO; 2) the $^1O_2$ has no effect on the formation of $^{\cdot}O_2^-$; and 3) the $^{\cdot}O_2^-$ play significant role in the formation of $^1O_2$.

Since the oxidation of $^{\cdot}O_2^-$ to $^1O_2$ (0.34 V vs NHE) is thermodynamically favored, the $^{\cdot}O_2^-$ can be oxidized by h^+ to $^1O_2$ [10]. To investigate the role of h^+ in the photocatalytic H_2O_2 production, the scavenger experiments using ammonium oxalate ($(NH_4)_2C_2O_4$) over g-C_3N_4-WO (Fig. S34A) and g-C_3N_4-CoWO (Fig. 8A) have been performed. The amounts of the formed H_2O_2 gradually increase with the increase of the $(NH_4)_2C_2O_4$ concentration in the reaction system because more e^- can be utilized for the O_2 reduction to H_2O_2 using $(NH_4)_2C_2O_4$ as the electron donor [35]. ESR analysis with TEMP as a spin-trapping reagent has been performed to investigate the role of h^+ in the formation of $^1O_2$ [10b]. Fig. 8B reveal that the signal intensity for the solution obtained by photoreaction over g-C_3N_4-CoWO gradually decreases with the addition of $(NH_4)_2C_2O_4$. The g-C_3N_4-WO has the same trend (Fig. S34B). The $^{\cdot}O_2^-$ concentration over g-C_3N_4-WO (Fig. S34C) and g-C_3N_4-CoWO (Fig. 8C) have been quantified with the addition of $(NH_4)_2C_2O_4$. The $^{\cdot}O_2^-$ concentrations over g-C_3N_4-WO and g-C_3N_4-CoWO increase with the increase of the $(NH_4)_2C_2O_4$ concentration in the reaction system because more e- can be utilized for the O_2 reduction to $^{\cdot}O_2^-$ using $(NH_4)_2C_2O_4$ as the electron donor [35]. ESR analysis with DMPO as a spin-trapping reagent has been performed to confirm the $^{\cdot}O_2^-$ concentration with the addition of $(NH_4)_2C_2O_4$ [8a]. Fig. 8D reveal that the signal intensity for the solution obtained by photoreaction over g-C_3N_4-CoWO gradually increase with the addition of $(NH_4)_2C_2O_4$. The g-C_3N_4-WO has the same trend (Fig. S34D). The $(NH_4)_2C_2O_4$ scavenger experiments and $^{\cdot}O_2^-$ quantitative experiments results combined with the ESR results reveal that $^{\cdot}O_2^-$ can be obtained through the single-electron O_2 reduction reaction and the $^{\cdot}O_2^-$ can be thus oxidized by h^+ to $^1O_2$.

Fig. 9A shows that g-C_3N_4-WO and g-C_3N_4-CoWO can produce almost the same amounts of H_2O_2 in water and ethanol. The electron-donating reaction can alternatively occur through the $^{\cdot}OH$-mediated process where $^{\cdot}OH$ forms as a result of H_2O or a surface-bound OH group reaction with a valence band hole and then reacts with organic electron donors through hydrogen abstraction [36]. The $^{\cdot}OH$ reaction pathway is important for compounds with α-hydrogens such as ethanol. The above results reveal that the ethanol is inefficient electron donors because $^{\cdot}OH$ formation is fairly small [35]. $^1O_2$ can undergo radiative decay around 1270 nm, and the

near-infrared emission was commonly used for determining quantum yields in solution [37]. Herein, by taking Rose Bengal (RB) as a standard photosensitizer, the $^1O_2$ quantum yields of g-C_3N_4-WO and g-C_3N_4-CoWO were evaluated by the formula of $\Phi_{Cat.} = \Phi_{RB}(I_{Cat.}/I_{RB})$. The integral areas of $^1O_2$ luminescence produced by g-C_3N_4-WO and g-C_3N_4-CoWO can be obtained through Fig. 9B. Based on the value for $\Phi_{RB} = 0.86$ in ethanol, Φ(g-C_3N_4-WO) and Φ(g-C_3N_4-CoWO) is estimated to be 0.89 and 0.64, respectively. The slightly shift of $^1O_2$ spectra between g-C_3N_4-WO and g-C_3N_4-CoWO and RB as shown in Fig. 9B may derive from their various surface environments, which is a common phenomenon in luminescence.[38] In order to quantify the $^1O_2$ concentration, 1,3-diphenylisobenzofuran (DPBF) has been used as the $^1O_2$ trapping agent [39]. Fig. 9C and D show the evolution of DPBF disappearance and the subsequent formation of $^1O_2$ during the photocatalytic H_2O_2 production of g-C_3N_4-WO and g-C_3N_4-CoWO in ethanol: 1) the g-C_3N_4-WO and g-C_3N_4-CoWO can produce the $^1O_2$ during the photocatalytic H_2O_2 production; 2) g-C_3N_4-CoWO produce the most $^1O_2$ among them. As shown in Figs. 9E and S38A, the amounts of H_2O_2 in ethanol have been found to be essentially the same as the amounts of formed $^1O_2$ in ethanol over g-C_3N_4-WO and g-C_3N_4-CoWO. The slope values of these above lines is close to 1, indicating that $^1O_2$ can proceed two-electron reduction to H_2O_2 [40]. To investigate the role of the $^{\cdot}O_2^-$ in the photocatalytic $^1O_2$ formation, the scavenger experiments for DPBF decomposition using PBQ over g-C_3N_4-WO (Fig. S38B) and g-C_3N_4-CoWO (Fig. S37) have been performed: the amounts of the formed $^1O_2$ gradually decrease with the increase of the PBQ concentration over g-C_3N_4-WO (Fig. S38C) and g-C_3N_4-CoWO (Fig. 9F). Combined with the above $(NH_4)_2C_2O_4$ scavenger experiments (Fig. 8A) and the ESR results (Fig. 8B), the PBQ scavenger experiments for $^1O_2$ results confirm that $^{\cdot}O_2^-$ can be obtained through the single-electron O_2 reduction reaction and the $^{\cdot}O_2^-$ can be thus oxidized by h^+ to $^1O_2$ [10].

The Mott-Schottky plots of g-C_3N_4, g-C_3N_4-Co, g-C_3N_4-WO and g-C_3N_4-CoWO at varied frequencies (1.0, 1.5 and 2.0 kHz) exhibit positive slopes (Fig. S39), suggestive of their n-type semiconductor features [41]. A flat band potential of -0.11, -0.25, -0.61 and -0.85 V vs. normal hydrogen electrode (NHE) has been obtained for g-C_3N_4, g-C_3N_4-Co, g-C_3N_4-WO and g-C_3N_4-CoWO, respectively [42]. In n-type semiconductors, the flat-band potential is approximately at the CB potential [43]. Therefore, the CB potentials of g-C_3N_4, g-C_3N_4-Co, g-C_3N_4-WO and g-C_3N_4-CoWO are -0.11, -0.25, -0.61 and -0.85 V vs. NHE. From the Tauc plots (Fig. S22C), the band gap of g-C_3N_4, g-C_3N_4-Co, g-C_3N_4-WO and g-C_3N_4-CoWO are 2.51, 2.48, 2.44 and 2.40 eV, respectively [44]. Combining the Mott-Schottky measurements and Tauc plots results, the valence band (VB) positions of g-C_3N_4, g-C_3N_4-Co, g-C_3N_4-WO and g-C_3N_4-CoWO have been estimated as 2.40, 2.23, 1.83 and 1.55 V vs. NHE, respectively (Fig. S40).

As shown in Fig. S40, a negative shift of 0.74 V for the CB level from g-C_3N_4 to g-C_3N_4-CoWO has been observed. The negative shift of the CB level in g-C_3N_4-CoWO can promote the e^- generation, which is consistent with the Koutecky-Levich plots and ESR-TEMPO results [6b,6c,34]. Moreover, the CB level in g-C_3N_4-CoWO (-0.85 V vs. NHE) has sufficient potential difference (0.72 V) from the single-electron reduction of O_2 to $^{\cdot}O_2$- (-0.13 V vs. NHE), confirming $^{\cdot}O_2$- quantitative and scavenger experiments results (Eq. (4)). The h^+ and $^1O_2$ scavenger experiments results demonstrate that $^{\cdot}O_2$- can be oxidized by h^+ to $^1O_2$ (0.34 V vs NHE, Eq. (6)) [10]. The $^1O_2$ quantitative experiments results indicate that the $^1O_2$ can proceed two-electron reduction to H_2O_2 [40] (Eq. (9)). The incorporation of CoWO into g-C_3N_4 framework can enhance the single-electron reduction of O_2 to $^{\cdot}O_2$- and furthermore promote the $^{\cdot}O_2$- oxidation to $^1O_2$ by h^+.

$$^1O_2 + 2H^+ + 2e^- \rightarrow H_2O_2 \quad (9)$$

3.4. Recycle of heterogeneous g-C_3N_4-CoWO

It is essential to confirm the catalysis of g-C_3N_4-CoWO is truly heterogeneous for photocatalytic H_2O_2 production. When the reaction time arrives at 30 min, g-C_3N_4-CoWO has been removed from the reaction system by filtration, and the reaction is allowed to proceed with the filtrate under the same conditions. As shown in Fig. S41A, no new H_2O_2 forms and the formed H_2O_2 starts to decompose under the same conditions. Furthermore, the ICP-AES result reveals no Co and W leaching in the filtrate. The above results rule out the contribution of Co and W species leached into the reaction solution for the observed catalytic results and confirms the g-C_3N_4-CoWO is truly heterogeneous for photocatalytic H_2O_2 production.

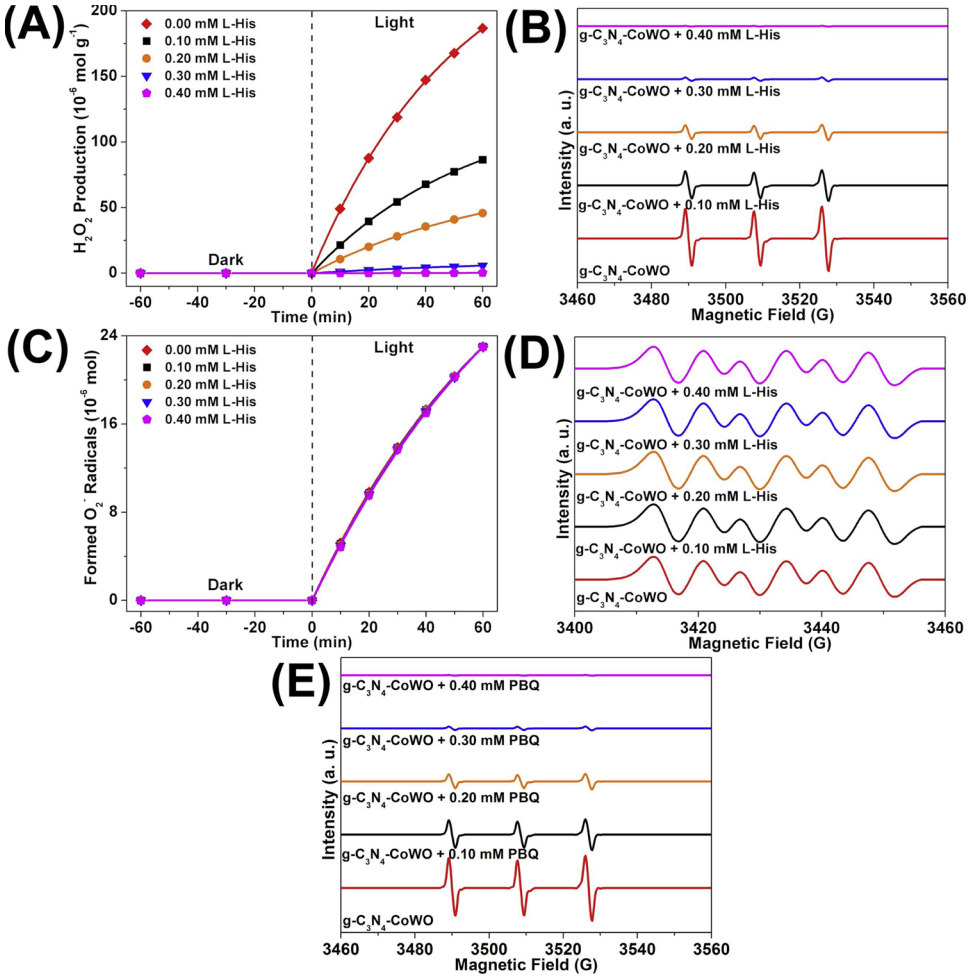

Fig. 7. The effect of L-His on the photocatalytic H_2O_2 production over g-C_3N_4-CoWO (A). Reaction conditions: water (100 ml), g-C_3N_4-CoWO (0.10 g, 1 g L^{-1}), L-His (0.10, 0.20, 0.30 and 0.40 mM), O_2-equilibrated, λ ≥ 420 nm, 25 °C. TEMP spin trapping ESR technique to measure $^1O_2$ generated photoreaction with the addition of L-His over g-C_3N_4-CoWO (B). The effect of L-His on $\cdot O_2^-$ formation during the photoreaction over g-C_3N_4-CoWO (C). Reaction conditions: water (100 ml), g-C_3N_4-CoWO (0.10 g, 1 g L^{-1}), L-His (0.10, 0.20, 0.30 and 0.40 mM), NBT (0.06 mM), O_2-equilibrated, λ ≥ 420 nm, 25 °C. DMPO spin trapping ESR technique to measure $\cdot O_2^-$ generated photoreaction with the addition of L-His over g-C_3N_4-CoWO (D). TEMP spin trapping ESR technique to measure $^1O_2$ generated photoreaction with the addition of PBQ over g-C_3N_4-CoWO (E).

To investigate the stability of heterogeneous g-C_3N_4-CoWO, the photocatalytic H_2O_2 production has been recycled for six times under the same conditions. Fig. S41B shows the catalytic performance is almost unchanged and the catalyst recovery can reach above 98% even after six times. The XRD and IR results of the fresh and used g-C_3N_4-CoWO exhibit almost the same typical peaks (Fig. S42). The STEM-Mapping results of the used g-C_3N_4-CoWO (Fig. S43) indicate that the sheet-like structure and the CoWO incorporated into g-C_3N_4 framework

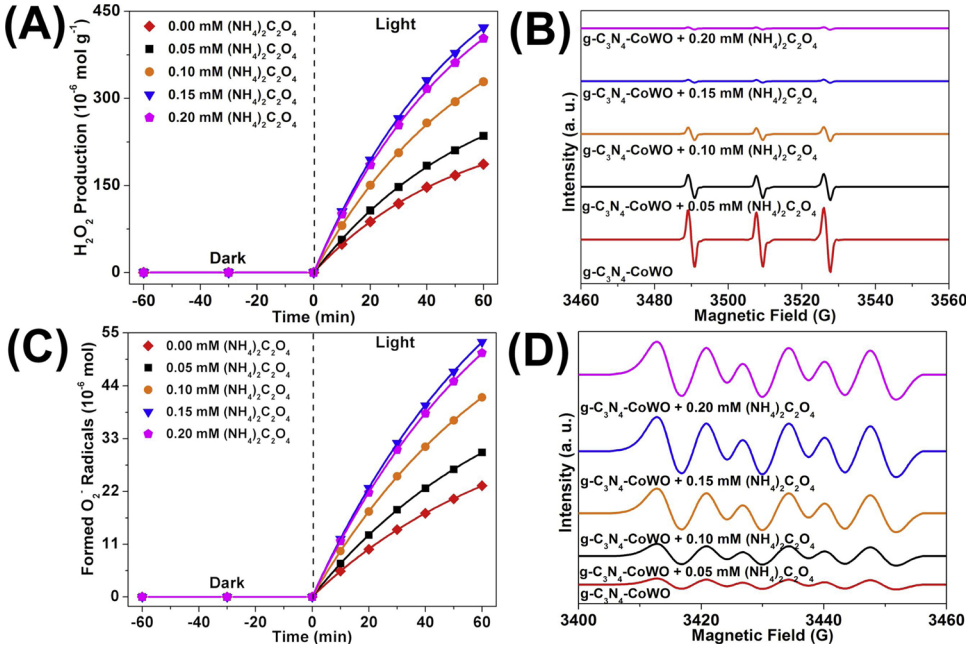

Fig. 8. The effect of $(NH_4)_2C_2O_4$ on the photocatalytic H_2O_2 production over g-C_3N_4-CoWO (A). Reaction conditions: water (100 ml), g-C_3N_4-CoWO (0.10 g, 1 g L^{-1}), $(NH_4)_2C_2O_4$ (0.05, 0.10, 0.15 and 0.20 mM), O_2-equilibrated, λ ≥ 420 nm, 25 °C. TEMP spin trapping ESR technique to measure $^1O_2$ generated photoreaction with the addition of $(NH_4)_2C_2O_4$ over g-C_3N_4-CoWO (B). The effect of $(NH_4)_2C_2O_4$ on $\cdot O_2^-$ formation during the photoreaction over g-C_3N_4-CoWO (C). Reaction conditions: water (100 ml), g-C_3N_4-CoWO (0.10 g, 1 g L^{-1}), $(NH_4)_2C_2O_4$ (0.05, 0.10, 0.15 and 0.20 mM), NBT (0.14 mM), O_2-equilibrated, λ ≥ 420 nm, 25 °C. DMPO spin trapping ESR technique to measure $\cdot O_2^-$ generated photoreaction with the addition of $(NH_4)_2C_2O_4$ over g-C_3N_4-CoWO (D).

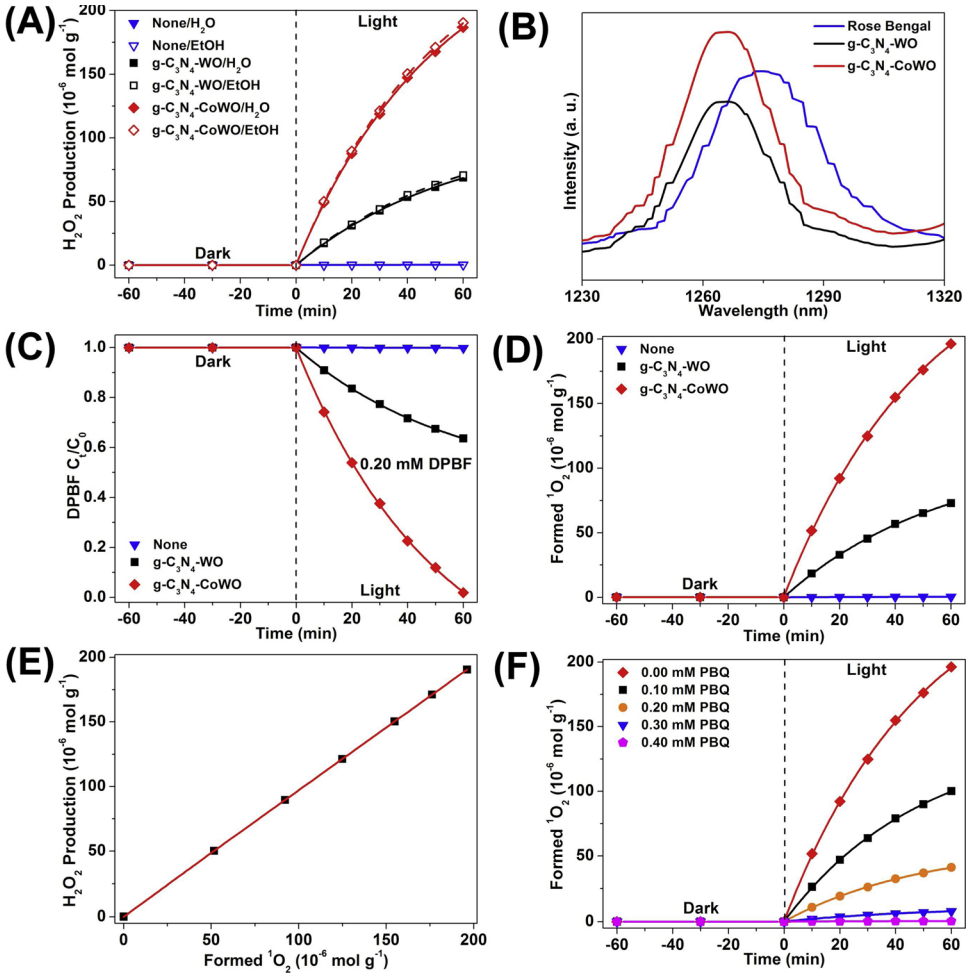

Fig. 9. Photocatalytic H_2O_2 formation over g-C_3N_4-WO and g-C_3N_4-CoWO in ethanol in 60 min (A). Reaction conditions: ethanol (100 ml), g-C_3N_4-WO or g-C_3N_4-CoWO (0.10 g, 1 g L^{-1}), O_2-equilibrated, $\lambda \geq 420$ nm, 25 °C. $^1O_2$ emission at ~1270 nm induced by the commercial Rose Bengal, g-C_3N_4-WO and g-C_3N_4-CoWO in ethanol under excitation with a 530 nm light (B). DPBF decomposition during the photoreaction over g-C_3N_4-WO and g-C_3N_4-CoWO in ethanol and the $^1O_2$ formation during the photoreaction over g-C_3N_4-WO and g-C_3N_4-CoWO in ethanol (D). Reaction conditions: ethanol (100 ml), g-C_3N_4-WO or g-C_3N_4-CoWO (0.10 g, 1 g L^{-1}), DPBF (0.20 mM), O_2-equilibrated, $\lambda \geq 420$ nm, 25 °C. Dependence of H_2O_2 formation on formed $^1O_2$ over g-C_3N_4-CoWO in ethanol (E) and $^1O_2$ formation during the photoreaction with the addition of PBQ over g-C_3N_4-CoWO in ethanol (F). Reaction conditions: ethanol (100 ml), g-C_3N_4-CoWO (0.10 g, 1 g L^{-1}), PBQ (0.10, 0.20, 0.30 and 0.40 mM), DPBF (0.20 mM), O_2-equilibrated, $\lambda \geq 420$ nm, 25 °C.

are retained after reaction. The EA and ICP results in Table S2 also reveal that the composition of the used g-C_3N_4-CoWO remains unchanged. The above results indicate that the heterogeneous g-C_3N_4-CoWO is catalytic stable.

4. Conclusions

In summary, to develop a new strategy of enhancing the h^+ consumption to promote the e^- utilization for O_2 reduction to H_2O_2 and maintaining the chemical stability of g-C_3N_4-based catalysts, the hybrid catalyst of g-C_3N_4-CoWO has been prepared through the calcination of the g-C_3N_4 precursor of 3-AT and the POMs precursor of NH_4-Co_2W_{12}. The hybrid catalyst of g-C_3N_4-CoWO with well-defined and stable structure exhibits efficient catalytic performance (9.7 μmol h^{-1}) for photocatalytic H_2O_2 production in the absence of organic electron donor under visible light. Four reasons have been presented for the efficient catalytic performance of g-C_3N_4-CoWO from the catalytic and characterization results: 1) the O_2-TPD and XPS O 1 s results reveal that the incorporation of CoWO into g-C_3N_4 framework can enhance the O_2 adsorption ability of CoWO; 2) the Koutecky-Levich plots and the ESR results suggest that the CoWO incorporated into g-C_3N_4 framework can promote the e^- generation for O_2 reduction; 3) the $^{\cdot}O_2$- quantitative and scavenger experiments results combined with the ESR results reveal that the negative shifts of the CB level from g-C_3N_4 to g-C_3N_4-CoWO can enhance the single-electron reduction of O_2 to $^{\cdot}O_2$-; and 4) the h^+ and $^1O_2$ scavenger experiments results combined with the ESR results demonstrate that the CoWO incorporated into g-C_3N_4 framework can promote the oxidation of $^{\cdot}O_2$- to $^1O_2$ by h^+. The $^1O_2$ quantitative experiments results indicate that the $^1O_2$ can proceed two-electron reduction to H_2O_2. The enhanced h^+ consumption and the $^1O_2$ transferred from $^{\cdot}O_2$- can promote the photocatalytic H_2O_2 production over g-C_3N_4-CoWO. In addition, the recycle experiment results reveal that the heterogeneous g-C_3N_4-CoWO is catalytic stable.

Acknowledgments

This work is supported by the National Natural Science Foundations of China (Grant Nos. 21777176, 21707154, 51578532) and the Chinese Academy of Sciences (QYZDB-SSW-DQC018).

Appendix A. Supplementary data

Supplementary material related to this article can be found, in the online version, at doi:https://doi.org/10.1016/j.apcatb.2019.02.031.

References

[1] (a) J.M. Campos-Martin, G. Blanco-Brieva, J.L.G. Fierro, Angew. Chem. 118 (2006) 7116–7139. Angew. Chem. Int. Ed. 45 (2006) 6962-6984;
(b) R. Hage, A. Lienke, Angew. Chem. 118 (2006) 212–229. Angew. Chem. Int. Ed. 45 (2006) 206-222;
(c) S.A. Mousavi Shaegh, N.T. Nguyen, S.M. Mousavi Ehteshami, S.H. Chan, Energy Environ. Sci. 5 (2012) 8225–8228.
[2] (a) F. Sandelin, P. Oinas, T. Salmi, J. Paloniemi, H. Haario, Ind. Eng. Chem. Res. 45 (2006) 986–992;
(b) J.K. Edwards, G.J. Hutchings, Angew. Chem. 120 (2008) 9332–9338. Angew. Chem. Int. Ed. 47 (2008) 9192-9198.
[3] (a) G.H. Moon, W. Kim, A.D. Bokare, N.E. Sung, W. Choi, Energy Environ. Sci. 7 (2014) 4023–4028;
(b) K. Mase, M. Yoneda, Y. Yamada, S. Fukuzumi, Nat. Comm. 7 (2016) 11470;
(c) M. Jakešová, D.H. Apaydin, M. Sytnyk, K. Oppelt, W. Heiss, N.S. Sariciftci,

E.D. Głowacki, Adv. Funct. Mater. 26 (2016) 5248–5254;
(d) S. Thakur, T. Kshetri, N.H. Kim, J.H. Lee, J. Catal. 345 (2017) 78–86;
(e) D. Shao, L. Zhang, S. Sun, W. Wang, ChemSusChem 11 (2018) 527–531;
(f) S. Fukuzumi, Y.M. Lee, W. Nam, Chem. Eur. J. 24 (2018) 5016–5031.
[4] (a) Y. Kofuji, Y. Isobe, Y. Shiraishi, H. Sakamoto, S. Tanaka, S. Ichikawa, T. Hirai, J. Am. Chem. Soc. 138 (2016) 10019–10025;
(b) S. Li, G. Dong, R. Hailili, L. Yang, Y. Li, F. Wang, Y. Zeng, C. Wang, Appl. Catal. B: Environ. 190 (2016) 26–35;
(c) H. Ou, P. Yang, L. Lin, M. Anpo, X. Wang, Angew. Chem. 129 (2017) 11045–11050. Angew. Chem. Int. Ed. 56 (2017) 10905-10910;
(d) L. Yang, G. Dong, D.L. Jacobs, Y. Wang, L. Zang, C. Wang, J. Catal. 352 (2017) 274–281.
[5] (a) Y. Kofuji, S. Ohkita, Y. Shiraishi, H. Sakamoto, S. Tanaka, S. Ichikawa, T. Hirai, ACS Catal. 6 (2016) 7021–7029;
(b) R. Wang, K. Pan, D. Han, J. Jiang, C. Xiang, Z. Huang, L. Zhang, X. Xiang, ChemSusChem 9 (2016) 2470–2479;
(c) S. Zhao, X. Zhao, H. Zhang, J. Li, Y. Zhu, Nano Energy 35 (2017) 405–414;
(d) Z. Wei, M. Liu, Z. Zhang, W. Yao, H. Tan, Y. Zhu, Energy Environ. Sci. 11 (2018) 2581–2589;
(e) Z. Zhu, H. Pan, M. Murugananthan, J. Gong, Y. Zhang, Appl. Catal. B: Environ. 232 (2018) 19–25.
[6] (a) O. Jung, M.L. Pegis, Z. Wang, G. Banerjee, C.T. Nemes, W.L. Hoffeditz, J.T. Hupp, C.A. Schmuttenmaer, G.W. Brudvig, J.M. Mayer, J. Am. Chem. Soc. 140 (2018) 4079–4084;
(b) S. Zhao, T. Guo, X. Li, T. Xu, B. Yang, X. Zhao, Appl. Catal. B: Environ. 224 (2018) 725–732;
(c) S. Zhao, X. Zhao, J. Catal. 366 (2018) 98–106;
(d) X. Guo, X. Li, X.C. Liu, P. Li, Z. Yao, J. Li, W. Zhang, J.P. Zhang, D. Xue, R. Cao, Chem. Commun. 54 (2018) 845–848.
[7] Y. Shiraishi, S. Kanazawa, Y. Kofuji, H. Sakamoto, S. Ichikawa, S. Tanaka, T. Hirai, Angew. Chem. 126 (2014) 13672–13677. Angew. Chem. Int. Ed. 53 (2014) 13454-13459.
[8] (a) Y. Shiraishi, Y. Kofuji, H. Sakamoto, S. Tanaka, S. Ichikawa, T. Hirai, ACS Catal. 5 (2015) 3058–3066;
(b) G.H. Moon, M. Fujitsuka, S. Kim, T. Majima, X. Wang, W. Choi, ACS Catal. 7 (2017) 2886–2895;
(c) Y. Zheng, Z. Yu, H. Ou, A.M. Asiri, Y. Chen, X. Wang, Adv. Funct. Mater. 28 (2018) 1705407;
(d) L. Shi, L. Yang, W. Zhou, Y. Liu, L. Yin, X. Hai, H. Song, J. Ye, Small 14 (2018) 1703142;
(e) S. Kim, G.H. Moon, H. Kim, Y. Mun, P. Zhang, J. Lee, W. Choi, J. Catal. 357 (2018) 51–58.
[9] J. Xiao, Q. Han, Y. Xie, J. Yang, Q. Su, Y. Chen, H. Cao, Environ. Sci. Technol. 51 (2017) 13380–13387.
[10] (a) D.T. Sawyer, Acc. Chem. Res. 14 (1981) 393–400;
(b) J.A. Rengifo-Herrera, K. Pierzchała, A. Sienkiewicz, L. Forró, J. Kiwi, C. Pulgarin, Appl. Catal. B: Environ. 88 (2009) 398–406;
(c) A.V. Demyanenko, A.S. Bogomolov, N.V. Dozmorov, A.I. Svyatova, A.P. Pyryaeva, V.G. Goldort, S.A. Kochubei, A.V. Baklanov, J. Phys. Chem. C 123 (2019) 2175–2181.
[11] (a) R.M. Cory, K. McNeill, J.P. Cotner, A. Amado, J.M. Purcell, A.G. Marshall, Environ. Sci. Technol. 44 (2010) 3683–3689;
(b) Y. Zhang, K.A. Simon, A.A. Andrew, R. Del Vecchio, N.V. Blough, Environ. Sci. Technol. 48 (2014) 12679–12688.
[12] (a) Y. Huang, J. Ge, J. Hu, J. Zhang, J. Hao, Y. Wei, Adv. Energy Mater. 8 (2018) 1701601;
(b) J. Hou, B. Zhang, Z. Li, S. Cao, Y. Sun, Y. Wu, Z. Gao, L. Sun, ACS Catal. 8 (2018) 4612–4621.
[13] L.C.W. Baker, T.P. McCutcheon, J. Am. Chem. Soc. 78 (1956) 4503–4510.
[14] G.P. Mane, S.N. Talapaneni, K.S. Lakhi, H. Ilbeygi, U. Ravon, K. Al-Bahily, T. Mori, D.H. Park, A. Vinu, Angew. Chem. 129 (2017) 8601–8605. Angew. Chem. Int. Ed. 56 (2017) 8481-8485.
[15] M. Teranishi, R. Hoshino, S.I. Naya, H. Tada, Angew. Chem. 128 (2016) 12965–12969. Angew. Chem. Int. Ed. 55 (2016) 12773-12777.
[16] G. He, J. Li, W. Li, B. Li, N. Noor, K. Xu, J. Hu, I.P. Parkin, J. Mater. Chem. A 3 (2015) 14272–14278.
[17] X. Wang, K. Maeda, A. Thomas, K. Takanabe, G. Xin, J.M. Carlsson, K. Domen, M. Antonietti, Nat. Mater. 8 (2009) 76–80.
[18] A. Thomas, A. Fischer, F. Goettmann, M. Antonietti, J.O. Müller, R. Schlögl, J.M. Carlsson, J. Mater. Chem. 18 (2008) 4893–4908.
[19] (a) J. Zhou, W. Chen, C. Sun, L. Han, C. Qin, M. Chen, X. Wang, E. Wang, Z. Su, ACS Appl. Mater. Interfaces 9 (2017) 11689–11695;
(b) H. Wang, C. Wang, Y. Yang, M. Zhao, Y. Wang, Catal. Sci. Technol. 7 (2017) 405–417.
[20] (a) Y. Zhu, M. Zhu, L. Kang, F. Yu, B. Dai, Ind. Eng. Chem. Res. 54 (2015) 2040–2047;
(b) H. Wang, M. Zhao, Q. Zhao, Y. Yang, C. Wang, Y. Wang, Ind. Eng. Chem. Res. 56 (2017) 2711–2721.
[21] Y. Sun, I. Sinev, W. Ju, A. Bergmann, S. Dresp, S. Kühl, C. Spöri, H. Schmies, H. Wang, D. Bernsmeier, B. Paul, R. Schmack, R. Kraehnert, B.R. Cuenya, P. Strasse, ACS Catal. 8 (2018) 2844–2856.
[22] J. Chen, W. Shi, X. Zhang, H. Arandiyan, D. Li, J. Li, Environ. Sci. Technol. 45 (2011) 8491–8497.
[23] C. Liu, L. Jing, L. He, Y. Luan, C. Li, Chem. Comm. 50 (2014) 1999–2001.
[24] X. Liu, A. Jin, Y. Jia, T. Xia, C. Deng, M. Zhu, C. Chen, X. Chen, Appl. Surf. Sci. 405 (2017) 359–371.
[25] S. Zhao, F. Hu, J. Li, ACS Catal. 6 (2016) 3433–3441.
[26] H. Huang, D.Y.C. Leung, ACS Catal. 1 (2011) 348–354.
[27] (a) J. Liu, S. Xie, Z. Geng, K. Huang, L. Fan, W. Zhou, L. Qiu, D. Gao, L. Ji, L. Duan, L. Lu, W. Li, S. Bai, Z. Liu, W. Chen, S. Feng, Y. Zhang, Nano Lett. 16 (2016) 6568–6575;
(b) S. Zhao, X. Zhao, S. Ouyang, Y. Zhu, Catal. Sci. Technol. 8 (2018) 1686–1695.
[28] Y. Su, L. Zhang, W. Wang, D. Shao, ACS Sustain. Chem. Eng. 6 (2018) 8704–8710.
[29] V. Maurino, C. Minero, G. Mariella, E. Pelizzetti, Chem. Commun. (2005) 2627–2629.
[30] (a) N. Kaynan, B.A. Berke, O. Hazut, R. Yerushalmi, J. Mater. Chem. A 2 (2014) 13822–13826;
(b) H.I. Kim, O.S. Kwon, S. Kim, W. Choi, J.H. Kim, Energy Environ. Sci. 9 (2016) 1063–1073.
[31] (a) H. Sheng, H. Ji, W. Ma, C. Chen, J. Zhao, Angew. Chem. 125 (2013) 9868–9872. Angew. Chem. Int. Ed. 52 (2013) 9686-9690;
(b) Y. Liu, H. Liu, C. Wang, S.X. Hou, N. Yang, Environ. Sci. Technol. 47 (2013) 13889–13895.
[32] W. He, H. Jia, J. Cai, X. Han, Z. Zheng, W.G. Wamer, J.J. Yin, J. Phys. Chem. C 120 (2016) 3187–3195.
[33] (a) S. Obregón, Y. Zhang, G. Colón, Appl. Catal. B: Environ. 184 (2016) 96–103;
(b) Z. Wei, D. Liu, W. Wei, X. Chen, Q. Han, W. Yao, X. Ma, Y. Zhu, ACS Appl. Mater. Interfaces 9 (2017) 15533–15540.
[34] (a) A.J. Hoffman, E.R. Carraway, M.R. Hoffmann, Environ. Sci. Technol. 28 (1994) 776–785;
(b) G.L. Chai, Z. Hou, T. Ikeda, K. Terakura, J. Phys. Chem. C 121 (2017) 14524–14533.
[35] W.C. Hou, Y.S. Wang, ACS Sustain. Chem. Eng. 5 (2017) 2994–3001.
[36] (a) E.R. Carraway, A.J. Hoffman, M.R. Hoffmann, Environ. Sci. Technol. 28 (1994) 786–793;
(b) W. Choi, M.R. Hoffmann, Environ. Sci. Technol. 29 (1995) 1646–1654.
[37] H. Wang, X. Yang, W. Shao, S. Chen, J. Xie, X. Zhang, J. Wang, Y. Xie, J. Am. Chem. Soc. 137 (2015) 11376–11382.
[38] (a) M. Kořinek, R. Dědic, A. Svoboda, J. Hála, J. Fluoresc. 14 (2004) 71–74;
(b) P. Bilski, B. Zhao, C.F. Chignell, Chem. Phys. Lett. 458 (2008) 157–160.
[39] J. Wang, D. Liu, Y. Zhu, S. Zhou, S. Guan, Appl. Catal. B: Environ. 231 (2018) 251–261.
[40] (a) G.G. Kramarenko, S.G. Hummel, S.M. Martin, G.R. Buettner, Photochem. Photobiol. 82 (2006) 1634–1637;
(b) S.A. Khorobrykh, M. Karonen, E. Tyystjärvi, FEBS Lett. 589 (2015) 779–786;
(c) H. Mattila, S. Khorobrykh, V. Havurinne, E. Tyystjärvi, J. Photochem. Photobiol. B: Biol. 152 (2015) 176–214.
[41] C. Zhao, H. Luo, F. Chen, P. Zhang, L. Yi, K. You, Energy Environ. Sci. 7 (2014) 1700–1707.
[42] R.L. Spray, K.J. McDonald, K.S. Choi, J. Phys. Chem. C 115 (2011) 3497–3506.
[43] K. Gelderman, L. Lee, S.W. Donne, J. Chem. Educ. 84 (2007) 685.
[44] (a) B. Li, Y. Zhao, S. Zhang, W. Gao, M. Wei, ACS Appl. Mater. Interfaces 5 (2013) 10233–10239;
(b) J. Liu, Y. Liu, N. Liu, Y. Han, X. Zhang, H. Huang, Y. Lifshitz, S.T. Lee, J. Zhong, Z. Kang, Science 347 (2015) 970–974.